Electronic Supplementary Information (ESI)

1. Materials and methods

1.1 Chemicals and measurement

All the chemicals and reagents were purchased from commercial sources and used as received without further purification. The end-products were collected via silica-gel column chromatography and then further purified via vacuum sublimation to be employed for PL and EL properties investigations. ^{1}H and ^{13}C NMR spectra were measured on a Bruker AV 400/500 spectrometer in CD_2Cl_2 or $CDCl_3$ at room temperature. High-resolution mass spectra (HRMS) were recorded on a GCT premier CAB048 mass spectrometer operating in MALDI-TOF mode. UV–vis absorption spectra were measured on a Shimadzu UV-2600 spectrophotometer. PL spectra were recorded on a Horiba Fluoromax-4 spectrofluorometer. PL quantum yields were measured using a Hamamatsu absolute PL quantum yield spectrometer C11347 Quantaurus QY. Temperature-dependent transient PL decay in films were measured in Edinburgh Instruments FLS1000 spectrometer. The prompt fluorescence lifetimes were measured by using time-correlated single photon counting (TCSPC) mode with a picosecond light source and delayed fluorescence lifetimes were measured by using multichannel scaling (MCS) mode with a variable pulse lasers (VPL) light source. Transient PL decay spectra of materials in solutions were measured using Quantaurus-Tau fluorescence lifetime measurement system (C11367-03, Hamamatsu Photonics Co., Japan). Thermal gravimetric analysis (TGA) data were collected from a TG209F1 under nitrogen protection at a heating rate of 20 K min^{-1}. Differential scanning calorimetric (DSC) analysis were performed on a DSC 214 Polymer under dry nitrogen at a heating rate of 10 °C min^{-1}. The ground-state geometries were optimized using the density function theory (DFT) method with B3LYP functional at the basis set level of 6-31G, and the ΔE_{ST} values between the S_1 and the T_1 were calculated by time-dependent DFT (TDDFT) method at the M062X/6-311G (d, p) level. All the calculations were performed using Gaussian16 package. Cyclic voltammogram was measured in a solution of tetra-*n*-butylammonium hexafluorophosphate (Bu_4NPF_6, 0.1 M) in dichloromethane and *N*, *N*-dimethylformamide (DMF) containing the sample at a scan rate of 100 mV s^{-1}. Three-electrode system (Ag/Ag^+, platinum wire and glassy carbon electrode as reference, counter and work electrode respectively) was used in the CV method. $E_{HOMO} = -[E_{ox} + 4.8]$ eV, and $E_{LUMO} = -[E_{re} + 4.8]$ eV. E_{ox} and E_{re} represent the onsets oxidation (measured in dichloromethane) and reduction (measured in DMF) potentials relative to ferrocene.

1.2 Device fabrication

Glass substrates pre-coated with a 95-nm-thin layer of indium tin oxide (ITO) with a sheet resistance of 20 Ω per square were thoroughly cleaned for 10 minutes in ultrasonic bath of acetone, isopropyl alcohol, detergent, deionized water, and isopropyl alcohol and then treated with O_2 plasma for 5 min in sequence in order to improve the hole injection ability. Organic layers were deposited onto the ITO-coated substrates by high-vacuum ($< 5 \times 10^{-4}$ Pa) thermal evaporation in the Fangsheng OMV-FS380 vacuum deposition system. Organic materials, Liq and Al were deposited at rates of 1~2 A s^{-1}, 0.1 A s^{-1} and 5 A s^{-1}, respectively. The emission area of the devices is 3 × 3 mm^2 as shaped by the overlapping area of the anode and cathode. All the device characterization steps were carried out at

room temperature under ambient laboratory conditions without encapsulation. The luminance–voltage–current density and EQE were characterized with a dual-channel Keithley 2614B source meter and a PIN-25D silicon photodiode. The EQEs were determined by assuming Lambertian pattern. The electroluminescence spectra were obtained via an Ocean Optics USB 2000+ spectrometer, along with a Keithley 2614B Source Meter. Simulated angle dependent relative luminance of the devices was taken by CS-200 Color and Luminance Meter.

2. Equations for photophysical properties

The quantum efficiencies and rate constants were determined using the following equations according to Adachi's method.[1–3]

$\Phi_{prompt} = \Phi_{PL} R_{prompt}$

$\Phi_{delayed} = \Phi_{PL} R_{delayed}$

$k_F = \Phi_{prompt}/\tau_{prompt}$

$\Phi_{PL} = k_F/(k_F + k_{IC})$

$\Phi_{prompt} = k_F/(k_F + k_{IC} + k_{ISC})$

$\Phi_{IC} = k_{IC}/(k_F + k_{IC} + k_{ISC})$

$\Phi_{ISC} = k_{ISC}/(k_F + k_{IC} + k_{ISC}) = 1 - \Phi_{prompt} - \Phi_{IC}$

$\Phi_{RISC} = \Phi_{delayed}/\Phi_{ISC}$

$k_{RISC} = (k_p k_d \Phi_{delayed})/(k_{ISC} \Phi_{prompt})$

$k_p = 1/\tau_{prompt}$; $k_d = 1/\tau_{delayed}$

3. Additional Figures and Tables

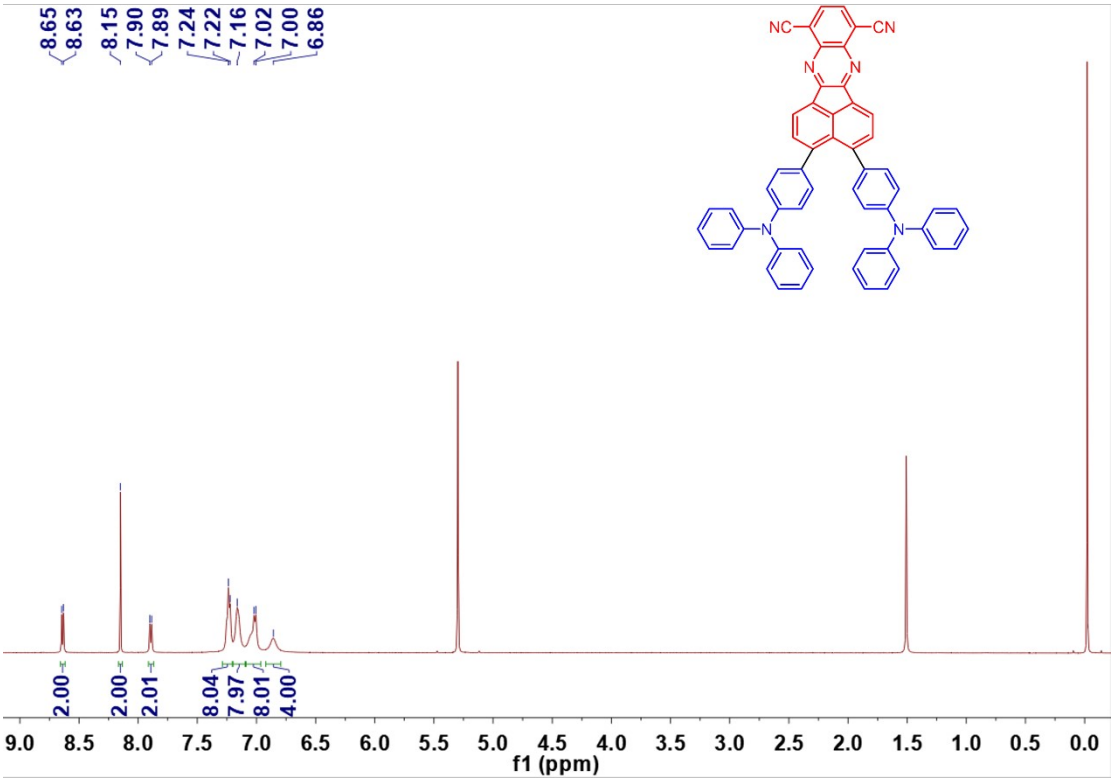
8.65
8.63
8.15
7.90
7.89
7.24
7.22
7.16
7.02
7.00
6.86
NC
CN
N
N
N
N
2.00
2.00
2.01
8.04
7.97
8.01
4.00
9.0 8.5 8.0 7.5 7.0 6.5 6.0 5.5 5.0 4.5 4.0 3.5 3.0 2.5 2.0 1.5 1.0 0.5 0.0
f1 (ppm)

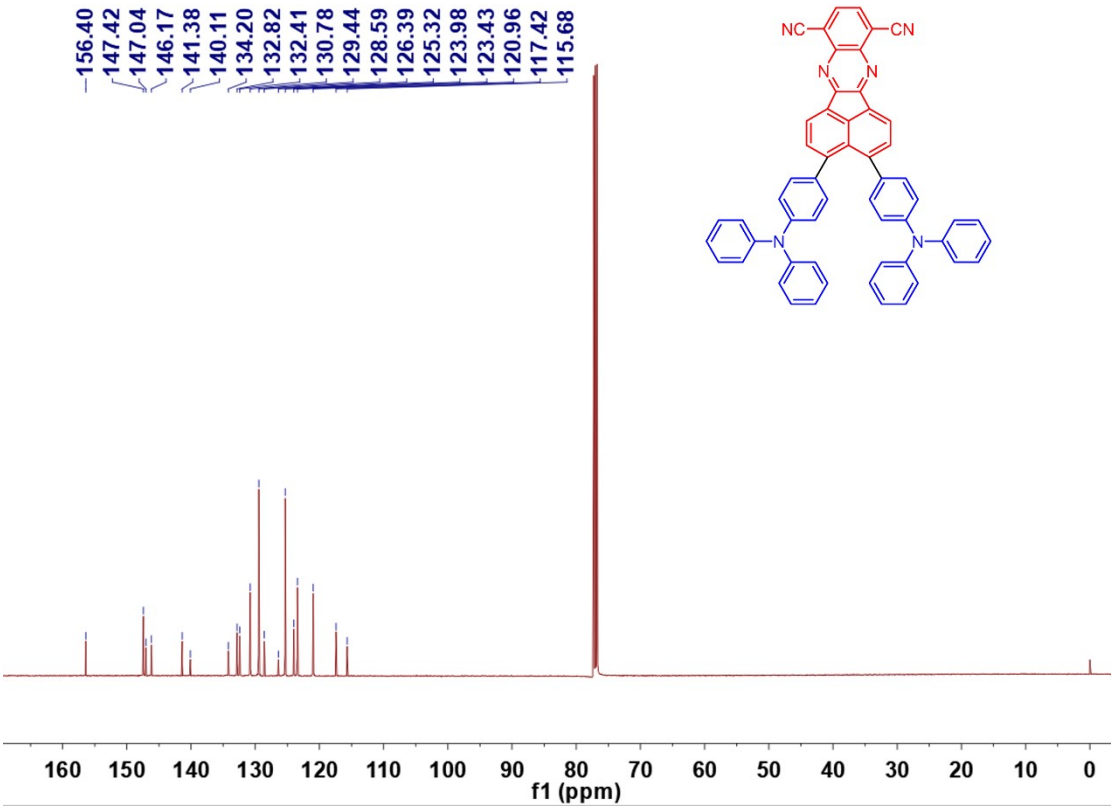
156.40
147.42
147.04
146.17
141.38
140.11
134.20
132.82
132.41
130.78
129.44
128.59
126.39
125.32
123.98
123.43
120.96
117.42
115.68
NC
CN
N
N
N
N
160 150 140 130 120 110 100 90 80 70 60 50 40 30 20 10 0
f1 (ppm)

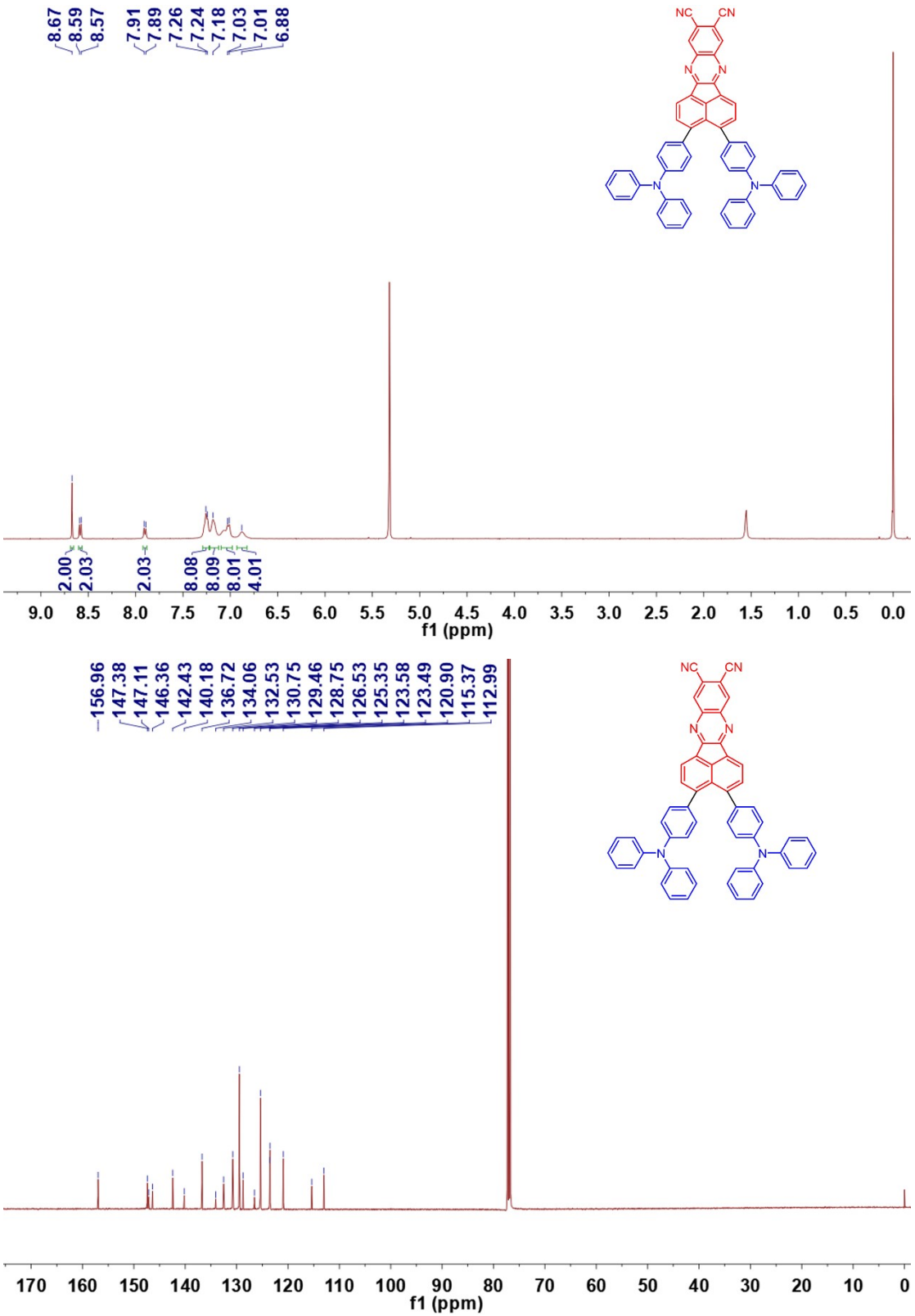

Fig. S1 NMR spectra of *p*-APDC-DTPA and *o*-APDC-DTPA, dissolving in dichloromethane-d_2 and chloroform.

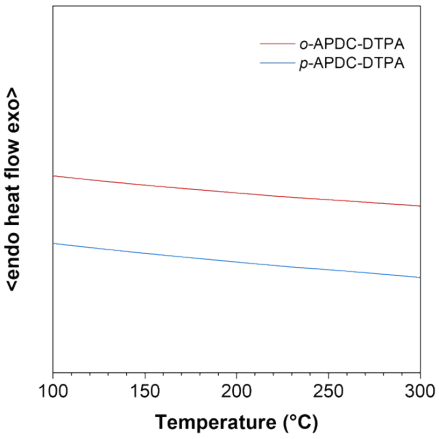

Fig. S2 DSC thermograms recorded under nitrogen at a heating rate of 10 °C min^{-1}.

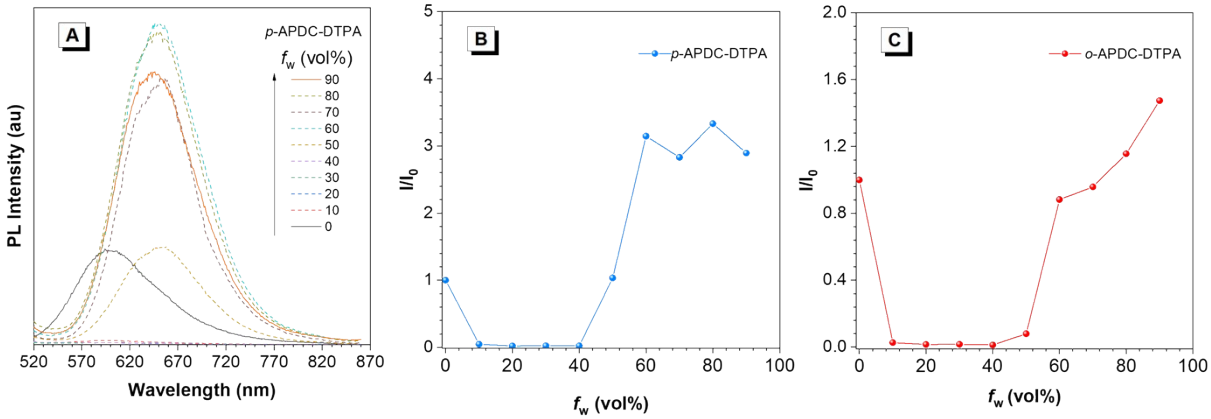

Fig. S3 (A)PL spectra of *p*-APDC-DTPA in THF/water mixtures with different water fractions (f_w). (B) Plots of I/I_0 values versus f_w of *p*-APDC-DTPA in THF/water mixtures. (C) Plots of I/I_0 values versus f_w of *o*-APDC-DTPA in THF/water mixtures. (I_0 is the PL intensity in pure THF, and I is the PL intensity in the mixtures).

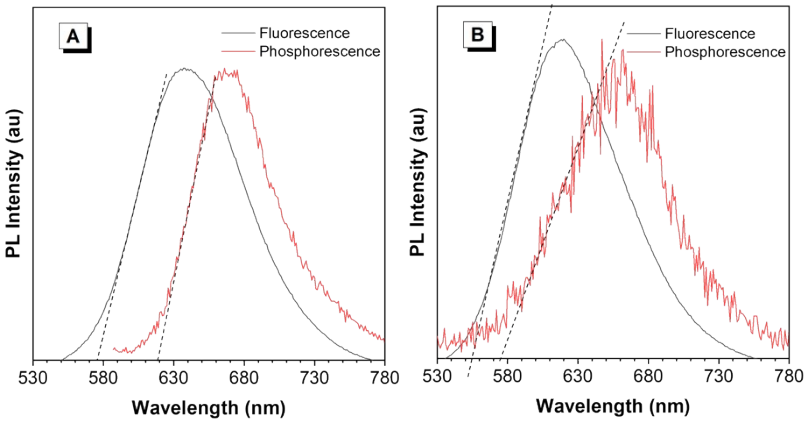

Fig. S4 Fluorescence and phosphorescence spectra of (A) *p*-APDC-DTPA and (B) *o*-APDC-DTPA doped in TPBi films with a concentration of 10 wt% measured at 77 K.

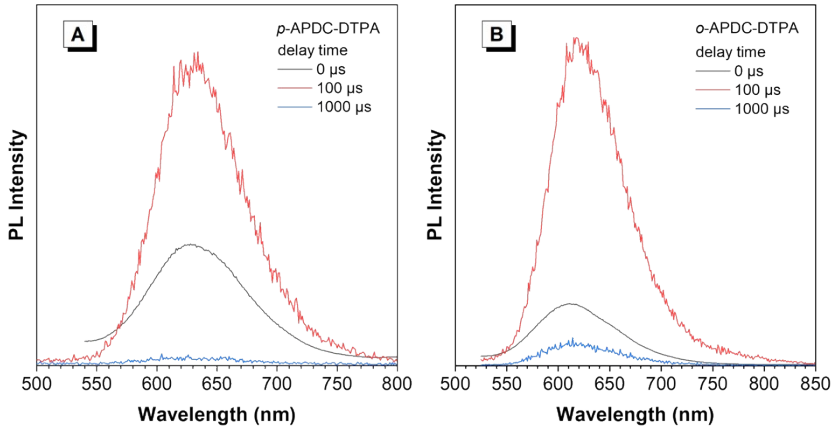

Fig. S5 PL spectra of (A) 10 wt% *p*-APDC-DTPA: TPBi doped film and (B) 10 wt% *o*-APDC-DTPA: TPBi doped film, measured with different delay times at room temperature.

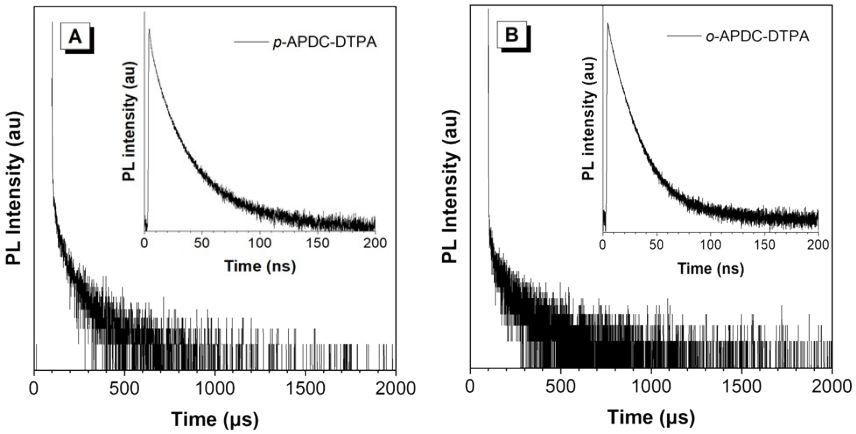

Fig. S6 Transient PL decay spectra of (A) *p*-APDC-DTPA and (B) *o*-APDC-DTPA doped in TPBi films with a concentration of 10 wt% measured at 300 K.

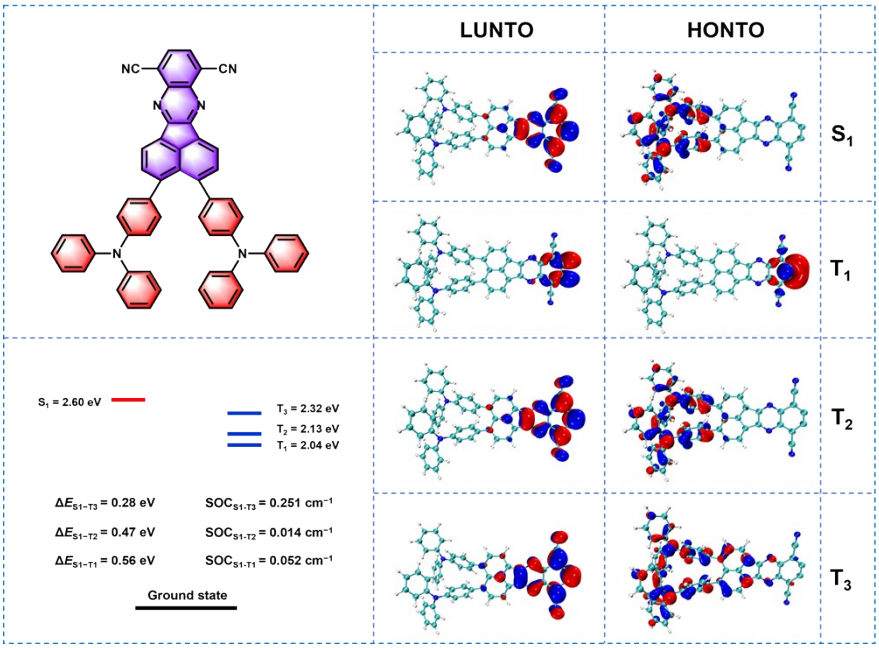

Fig. S7 The NTO analyses of excited singlet and triplet states of *p*-APDC-DTPA with the SOC matrix elements. Calculated energy levels, ΔE_{ST} values, and SOC matrix elements of excited singlet and

triplet states of *p*-APDC-DTPA.

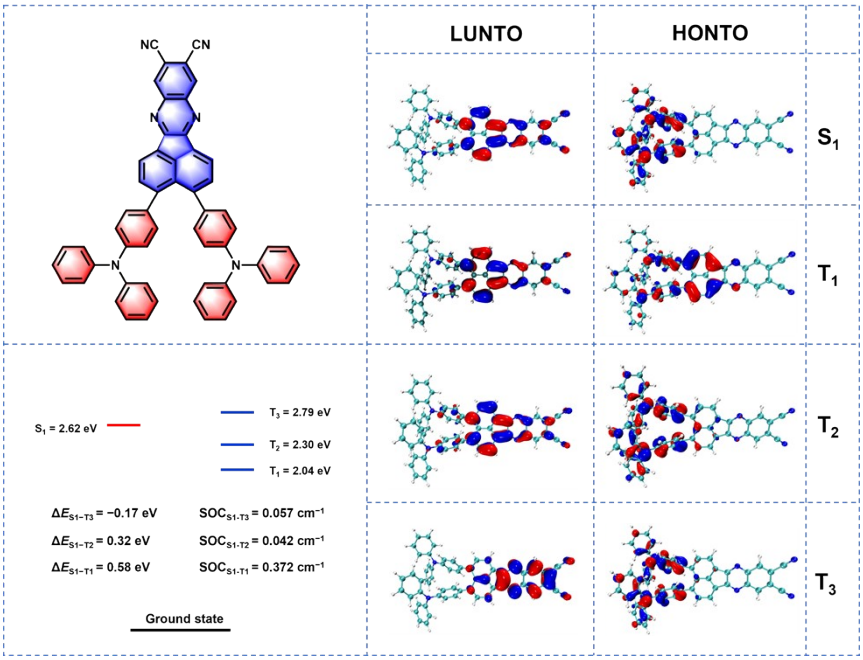

Fig. S8 The NTO analyses of excited singlet and triplet states of *o*-APDC-DTPA with the SOC matrix elements. Calculated energy levels, ΔE_{ST} values, and SOC matrix elements of excited singlet and triplet states of *o*-APDC-DTPA.

Table S1. Temperature-dependent photophysical parameters of doped films in TPBi host with a concentration of 10 wt%.

	Temperature (K)	*p*-APDC-DTPA	*o*-APDC-DTPA
$\tau_{delayed}$ (μs)	300	69.16	69.50
	250	64.16	80.23
	200	87.77	49.61
	150	54.90	35.97
	100	5.20	21.34
	77	6.25	10.17
$R_{delayed}$ (%)	300	62	63
	250	55	43
	200	36	3
	150	13	3
	100	4	1
	77	3	1

a) $\tau_{delayed}$ = lifetimes calculated from delayed fluorescence decay; $R_{delayed}$ = ratio of delayed component.

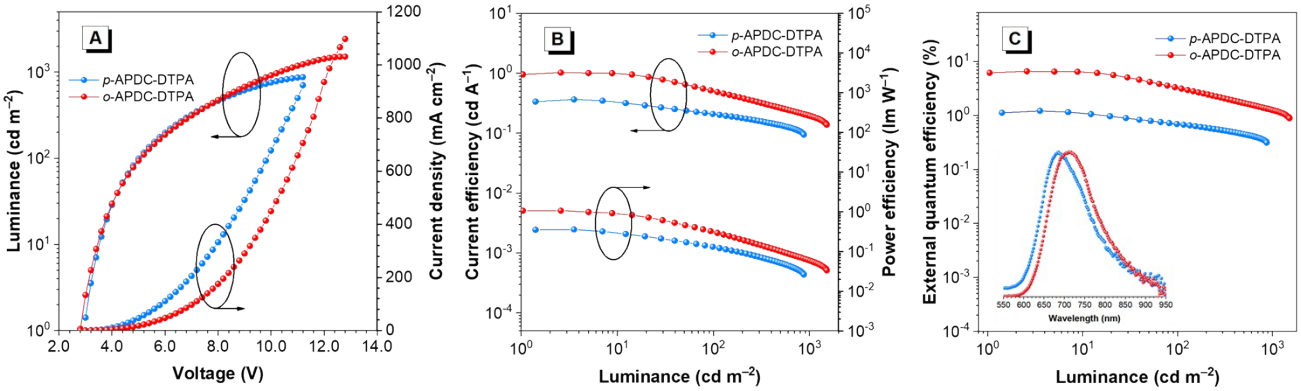

Fig. S9. A) Luminance–voltage–current density, B) current efficiency–luminance–power efficiency and C) external quantum efficiency–luminance of the non-doped OLEDs. Inset in plane E: EL spectra of the non-doped OLEDs.

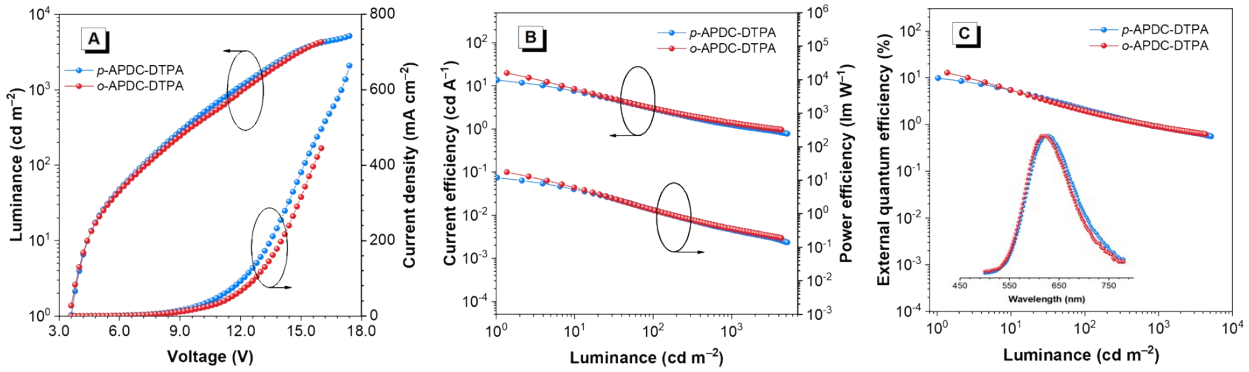

Fig. S10 A) luminance–voltage–current density, B) current efficiency–luminance–power efficiency and C) external quantum efficiency–luminance of the doped OLEDs with the concentration of 5 wt% in TPBi. Inset in plane E: EL spectra of the doped OLEDs.

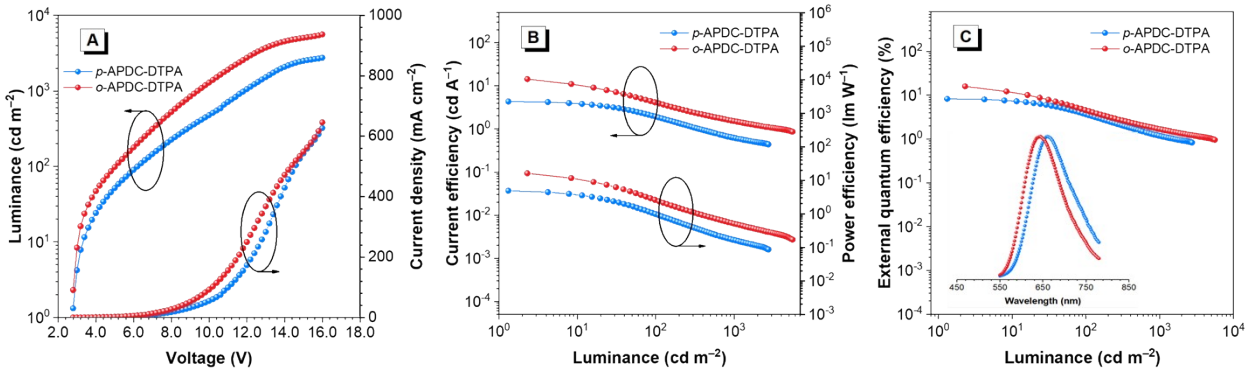

Fig. S11 A) luminance–voltage–current density, B) current efficiency–luminance–power efficiency and C) external quantum efficiency–luminance of the doped OLEDs with the concentration of 15 wt% in TPBi. Inset in plane E: EL spectra of the doped OLEDs.

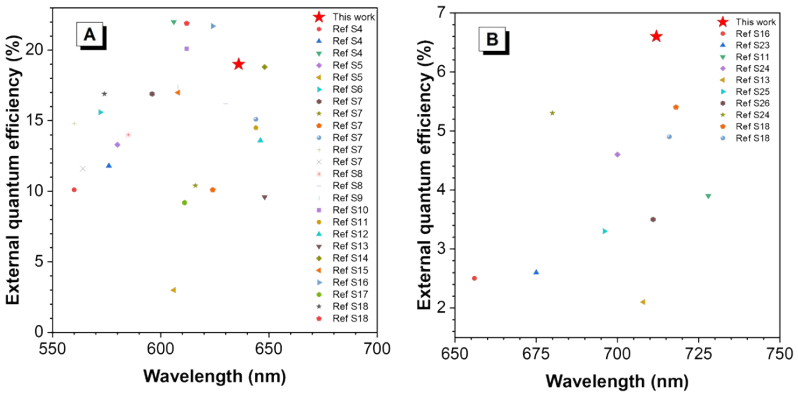

Fig. S12 A) EQE summary based on the dicyanopyrazino phenanthrene core. B) EQE summary of representative non-doped red/NIR TADF-OLEDs with emission peaks from 650 to 750 nm.

Table S2. The EL performance based phenanthrene core and non-doped deep-red/NIR emitters with emission peaks above 600 nm.

Emitter	Year	λ_{EL} (nm)	EQE (%)	CIE (x, y)	Ref.
3,6APDC-DTPA	2022	636	10.5	(0.62, 0.38)	This work
4,5APDC-DTPA	2022	636	19.0	(0.63, 0.37)	This work
1DMAC-BP	2019	560	10.1	(0.43, 0.54)	4
2DMAC-BP	2019	576	11.8	(0.43, 0.54)	4
3DMAC-BP	2019	606	22.0	(0.43, 0.54)	4
Ac-CNP	2016	580	13.3	(0.47, 0.51)	5
Px-CNP	2016	606	3.0	(0.53, 0.44)	5
PyCN-ACR	2016	572	15.6	(0.46, 0.52)	6
DMAC-Ph-DCPP	2017	596	16.9	(0.53, 0.46)	7
DPA-DCPP	2017	616	10.4	(0.61, 0.38)	7
DMAC-DCPP	2017	624	10.1	(0.60, 0.40)	7
DPA-Ph-DCPP	2017	644	15.1	(0.64, 0.36)	7
Cz-DCPP	2017	560	14.8	(0.44, 0.54)	7
Cz-Ph-DCPP	2017	564	11.6	(0.46, 0.52)	7
Ac-CNBQx	2018	585	14.0	(0.51, 0.48)	8
Ac-CNBPz	2018	630	16.2	(0.61, 0.39)	8
Da-CNBQx	2018	617	20.0	(0.59, 0.41)	8
PXZ-DCPP	2018	608	17.4	(0.56, 0.43)	9
DPXZ-BPPZ	2018	612	20.1	(0.60, 0.40)	10
TPA-QCN	2017	644	14.5	(0.62, 0.38)	11
DDTPACz-DCPP	2019	646	13.6	(0.61, 0.38)	12
TPA-DCPP	2015	648	9.6	(0.64, 0.35)	13
TPA-PPDCN	2019	648	18.8	(0.65, 0.35)	14
tDBBPZ-DPXZ	2019	608	17.0	(0.57, 0.43)	15
DBPZ-PDXZ	2019	608	17.8	(0.58, 0.42)	15
mDPBPZ-PXZ	2019	624	21.7	(0.62, 0.38)	16
TAT-DBPZ	2020	604	15.4	-	17
TAT-FDBPZ	2020	611	9.2	-	17

TCQ	2022	574	16.9	(0.48, 0.50)	18
TCPQ	2022	612	21.9	(0.58, 0.41)	18
TPQ	2022	622	21.8	(0.62, 0.39)	18
ANQDC-MeFAC	2020	614	26.3	(0.60, 0.40)	19
ANQDC-DMAC	2020	615	27.5	(0.58, 0.41)	19
T-DA-2	2020	640	26.3	(0.62, 0.37)	20
TPA-PZCN	2019	648	28.1	(0.66, 0.34)	21
DCPPr-α-NDPA	2021	606	31.5	(0.58, 0.42)	22
4,5APDC-DTPA	2022	712	6.6	(0.69, 0.29)	This work
mDPBPZ-PXZ	2019	680	5.2	(0.68, 0.32)	16
BPPZ-PXZ	2019	656	2.5	(0.65, 0.35)	16
TPATCN	2015	675	2.6	(0.67, 0.32)	23
TPA-QCN	2017	728	3.9	(0.69, 0.31)	11
pCNQ-TPA	2021	700	4.6	-	24
TPA-DCPP	2015	708	2.1	(0.70, 0.29)	13
NZ2TPA	2017	696	3.3	(0.70, 0.30)	25
TAPPQ	2019	711	3.5	-	26
TPA-PZCN	2019	680	5.3	(0.69, 0.30)	21
TCPQ	2022	718	5.4	(0.70, 0.30)	18
TPQ	2022	716	4.9	(0.69, 0.30)	18

Table S3. EL performances of the OLEDs based on *p*-APDC-DTPA and *o*-APDC-DTPA fabricated with device structure of ITO/HATCN (5 nm)/NPB (30 nm)/mCP (5 nm)/EML (20 nm)/TPBi (50 nm)/LiF (1 nm)/Al.

Emitter	concentration	V_{on}[a)] (V)	L_{max} (cd m^{-2})	CE (cd A^{-1})	PE (lm W^{-1})	EQE (%)	λ_{EL} (nm)	CIE (x, y)
p-APDC-DTPA	5%	3.2	2593	4.3	3.7	4.2	634	(0.615, 0.376)
	10%	2.8	2645	3.3	3.4	5.3	658	(0.651, 0.343)
	15%	2.8	2598	2.3	2.5	5.1	668	(0.668, 0.327)
o-APDC-DTPA	5%	3.0	5912	11.8	11.3	6.4	610	(0.561, 0.430)
	10%	2.8	5252	13.7	14.6	11.0	628	(0.610, 0.386)
	15%	2.8	5319	11.3	12.7	11.2	640	(0.628, 0.369)

[a)] Abbreviations: V_{on} = turn-on voltage at 1 cd m^{-2}; L_{max} = maximum luminance; CE = maximum current efficiency; PE = maximum power efficiency; EQE = maximum external quantum efficiency; λ_{EL} = electroluminescence peak; CIE = Commission Internationale de I'Eclairage coordinates.

References

1. Q. Zhang, H. Kuwabara, W. J. Potscavage, Jr., S. Huang, Y. Hatae, T. Shibata and C. Adachi, Anthraquinone-based intramolecular charge-transfer compounds: computational molecular design, thermally activated delayed fluorescence, and highly efficient red electroluminescence，*J. Am. Chem. Soc.*, 2014, **136**, 18070-18081.
2. G. Xie, X. Li, D. Chen, Z. Wang, X. Cai, D. Chen, Y. Li, K. Liu, Y. Cao and S. J. Su, Evaporation- and solution-process-feasible highly efficient thianthrene-9,9′,10,10′-tetraoxide-based thermally activated delayed fluorescence emitters with reduced efficiency roll-off, *Adv. Mater.*, 2016, **28**,

181-187.
3. H. Uoyama, K. Goushi, K. Shizu, H. Nomura and C. Adachi, Highly efficient organic light-emitting diodes from delayed fluorescence, *Nature*, 2012, **492**, 234-238.
4. F. M. Xie, H. Z. Li, G. L. Dai, Y. Q. Li, T. Cheng, M. Xie, J. X. Tang and X. Zhao, Rational molecular design of dibenzo[*a*,*c*]phenazine-based thermally activated delayed fluorescence emitters for orange-red OLEDs with EQE up to 22.0%, *ACS Appl. Mater. Interfaces*, 2019, **11**, 26144-26151.
5. I. S. Park, S. Y. Lee, C. Adachi and T. Yasuda, Full-color delayed fluorescence materials based on wedge-shaped phthalonitriles and dicyanopyrazines: systematic design, tunable photophysical properties, and OLED performance, *Adv. Funct. Mater.*, 2016, **26**, 1813-1821.
6. X. Cai, X. Li, G. Xie, Z. He, K. Gao, K. Liu, D. Chen, Y. Cao and S. J. Su, "Rate-limited effect" of reverse intersystem crossing process: the key for tuning thermally activated delayed fluorescence lifetime and efficiency roll-off of organic light emitting diodes, *Chem. Sci.*, 2016, **7**, 4264-4275.
7. S. Wang, Z. Cheng, X. Song, X. Yan, K. Ye, Y. Liu, G. Yang and Y. Wang, Highly efficient long-wavelength thermally activated delayed fluorescence OLEDs based on dicyanopyrazino phenanthrene derivatives, *ACS Appl. Mater. Interfaces*, 2017, **9**, 9892-9901.
8. R. Furue, K. Matsuo, Y. Ashikari, H. Ooka, N. Amanokura and T. Yasuda, Highly efficient red–orange delayed fluorescence emitters based on strong π-accepting dibenzophenazine and dibenzoquinoxaline cores: toward a rational pure-red OLED design, *Adv. Opt. Mater.*, 2018, **6**, 1701147.
9. B. Wang, X. Qiao, Z. Yang, Y. Wang, S. Liu, D. Ma and Q. Wang, Realizing efficient red thermally activated delayed fluorescence organic light-emitting diodes using phenoxazine/phenothiazine-phenanthrene hybrids, *Org. Electron.*, 2018, **59**, 32-38.
10. J. X. Chen, K. Wang, C. J. Zheng, M. Zhang, Y. Z. Shi, S. L. Tao, H. Lin, W. Liu, W. W. Tao, X. M. Ou and X. H. Zhang, Red organic light-emitting diode with external quantum efficiency beyond 20% based on a novel thermally activated delayed fluorescence emitter, *Adv. Sci.*, 2018, **5**, 1800436.
11. C. Li, R. Duan, B. Liang, G. Han, S. Wang, K. Ye, Y. Liu, Y. Yi and Y. Wang, Deep-red to near-infrared thermally activated delayed fluorescence in organic solid films and electroluminescent devices, *Angew. Chem. Int. Ed.*, 2017, **56**, 11525-11529.
12. B. Wang, H. Yang, Y. Zhang, G. Xie, H. Ran, T. Wang, Q. Fu, Y. Ren, N. Sun, G. Zhao, J.-Y. Hu and Q. Wang, Highly efficient electroluminescence from evaporation- and solution-processable orange–red thermally activated delayed fluorescence emitters, *J. Mater. Chem. C*, 2019, **7**, 12321-12327.
13. S. Wang, X. Yan, Z. Cheng, H. Zhang, Y. Liu and Y. Wang, Highly efficient near-infrared delayed fluorescence organic light emitting diodes using a phenanthrene-based charge-transfer compound, *Angew. Chem. Int. Ed.*, 2015, **54**, 13068-13072.
14. T. Yang, B. Liang, Z. Cheng, C. Li, G. Lu and Y. Wang, Construction of efficient deep-red/near-infrared emitter based on a large π-conjugated acceptor and delayed fluorescence OLEDs with external quantum efficiency of over 20%, *The J. Phys. Chem. C*, 2019, **123**, 18585-18592.
15. J. X. Chen, W. W. Tao, Y. F. Xiao, K. Wang, M. Zhang, X. C. Fan, W. C. Chen, J. Yu, S. Li, F. X. Geng, X. H. Zhang and C. S. Lee, Efficient orange-red thermally activated delayed fluorescence emitters feasible for both thermal evaporation and solution process, *ACS Appl.*

Mater. Interfaces, 2019, **11**, 29086-29093.
16. J. X. Chen, W. W. Tao, W. C. Chen, Y. F. Xiao, K. Wang, C. Cao, J. Yu, S. Li, F. X. Geng, C. Adachi, C. S. Lee and X. H. Zhang, Red/near-infrared thermally activated delayed fluorescence OLEDs with near 100 % internal quantum efficiency, *Angew. Chem. Int. Ed.*, 2019, **58**, 14660-14665.
17. Y. Liu, Y. Chen, H. Li, S. Wang, X. Wu, H. Tong and L. Wang, High-performance solution-processed red thermally activated delayed fluorescence OLEDs employing aggregation-induced emission-active triazatruxene-based emitters, *ACS Appl. Mater. Interfaces*, 2020, **12**, 30652-30658.
18. Y. Liu, J. Yang, Z. Mao, X. Chen, Z. Yang, X. Ge, X. Peng, J. Zhao, S. J. Su and Z. Chi, Asymmetric thermally activated delayed fluorescence emitter for highly efficient red/near-infrared organic light-emitting diodes, *ACS Appl. Mater. Interfaces*, 2022, **14**, 33606–33613.
19. X. Gong, P. Li, Y. H. Huang, C. Y. Wang, C. H. Lu, W. K. Lee, C. Zhong, Z. Chen, W. Ning, C. C. Wu, S. Gong and C. Yang, A red thermally activated delayed fluorescence emitter simultaneously having high photoluminescence quantum efficiency and preferentially horizontal emitting dipole orientation, *Adv. Funct. Mater.*, 2020, **30**, 1908839.
20. T. Yang, Z. Cheng, Z. Li, J. Liang, Y. Xu, C. Li and Y. Wang, Improving the efficiency of red thermally activated delayed fluorescence organic light-emitting diode by rational isomer engineering, *Adv. Funct. Mater.*, 2020, **30**, 2002681.
21. Y. L. Zhang, Q. Ran, Q. Wang, Y. Liu, C. Hanisch, S. Reineke, J. Fan and L. S. Liao, High-efficiency red organic light-emitting diodes with external quantum efficiency close to 30% based on a novel thermally activated delayed fluorescence emitter, *Adv. Mater.*, 2019, **31**, 1902368.
22. Z. Cai, X. Wu, H. Liu, J. Guo, D. Yang, D. Ma, Z. Zhao and B. Z. Tang, Realizing record-high electroluminescence efficiency of 31.5 % for red thermally activated delayed fluorescence molecules, *Angew. Chem. Int. Ed.*, 2021, **60**, 23635-23640.
23. X. Han, Q. Bai, L. Yao, H. Liu, Y. Gao, J. Li, L. Liu, Y. Liu, X. Li, P. Lu and B. Yang, Highly efficient solid-state near-infrared emitting material based on triphenylamine and diphenylfumaronitrile with an EQE of 2.58% in nondoped organic light-emitting diode, *Adv. Funct. Mater.*, 2015, **25**, 7521-7529.
24. Z. Li, D. Yang, C. Han, B. Zhao, H. Wang, Y. Man, P. Ma, P. Chang, D. Ma and H. Xu, Optimizing charge transfer and out-coupling of a quasi-planar deep-red TADF emitter: towards Rec.2020 gamut and external quantum efficiency beyond 30 %, *Angew. Chem. Int. Ed.*, 2021, **60**, 14846-14851.
25. T. Liu, L. Zhu, C. Zhong, G. Xie, S. Gong, J. Fang, D. Ma and C. Yang, Naphthothiadiazole-based near-infrared emitter with a photoluminescence quantum yield of 60% in neat film and external quantum efficiencies of up to 3.9% in nondoped OLEDs, *Adv. Funct. Mater.*, 2017, **27**, 1606384.
26. J. Xue, Q. Liang, R. Wang, J. Hou, W. Li, Q. Peng, Z. Shuai and J. Qiao, Highly efficient thermally activated delayed fluorescence via J-aggregates with strong intermolecular charge transfer, *Adv. Mater.*, 2019, **31**, 1808242.